Computers in Biology and Medicine 106 (2019) 140–148

Contents lists available at ScienceDirect

Computers in Biology and Medicine

journal homepage: www.elsevier.com/locate/compbiomed

Novel cone-and-plate flow chamber with controlled distribution of wall fluid shear stress

Chongyang Ye, Shahid Ali, Qing Sun, Mengmeng Guo, Yixuan Liu, Yan Gao, Bo Huo*

Department of Mechanics, School of Aerospace Engineering, Beijing Institute of Technology, Beijing, 100081, PR China

ARTICLE INFO

Keywords:
Cone-and-plate chamber
Fluid shear stress
Six-well culture plate
Finite element method
Particle image velocimetry

ABSTRACT

Fluid flow in blood vessels or interstitial fluid flow within tissue cavities plays important roles in tissue regeneration. One of the fundamental issues for *in vitro* study of the effects of fluid shear stress (FSS) on cells is the development of a flow chamber that can provide a controlled FSS field. In this study, we developed a novel cone-and-plate flow chamber based on viscometry technology, in which the cone's shape was optimized to produce a uniform wall FSS field on the surface of a standard six-well cell culture plate. By using a FSS finite element method, the effects of different geometric parameters of cone and plate, viscosity coefficient of fluid, and angular velocity on wall FSS at the bottom surface of the culture plate were investigated. Results of the simulation demonstrated that the cone with polyline or truncated generatrix (TG) could produce wall FSS as high as 1 or 2 Pa with uniform distribution, in which the area of the identical region for the cone with TG accounts for more than 69% of the total area. In addition, with the cone in close proximity to the plate surface, a gap distance of 0.1 mm can produce a uniform FSS field with a magnitude as high as 2 Pa over the majority of the plate. Furthermore, particle image velocimetry was utilized to measure the distribution of wall FSS, through which the numerical simulation results were experimentally demonstrated. This study presents a powerful new device for *in vitro* fluid flow loading at the cellular level.

1. Introduction

Fluid flow is one of the vital mechanical factors regulating the biological behaviors of blood cells, such as adhesion, migration, proliferation, and differentiation. For example, wall fluid shear stress (FSS), which is caused by the flow of blood against the endothelial cells of the blood vessel, plays an important role in regulating blood coagulation, vasomotor tone, and endothelial–immune cell interactions [1]. Additionally, FSS has been demonstrated to promote osteogenic lineage commitment of mesenchymal stem cells to further stimulate bone formation or repair [2]. The *in vivo* fluid flow in blood vessels or within bone cavities is very difficult to observe [3,4], thus developing *in vitro* loading devices to exert and observe fluid flow on cells is necessary.

One of the most commonly used devices to simulate FSS is the parallel-plate flow chamber. It is a traditional loading device that produces shear stress on the substrate, with the fluid flow driven by a peristaltic pump. This equipment has been extensively used to observe the biological responses of various kinds of cells [5,6,7]. The advantages of a parallel-plate flow chamber include its convenient application under a microscope and the ability to accurately control wall FSS on cells. However, this device may not be suitable in experiments where long-term fluid loading is required due to its tedious operational procedures and high occurrence of cell contamination [8].

The cone-and-plate viscometer has been used to conduct rheological measurements on non-Newtonian liquids since the 1930s [9]. This instrument consists of a rotating cone with a narrow angle in close proximity to a stationary flat plate. According to fluid mechanics, the shear rate between the cone and the plate is constant at any given rotational speed, as the primary flow moves along the circumferential direction. The secondary flow phenomenon, i.e., the radial component of motion in the cone-and-plate flow, was first observed by Cox using a dye-visualization technique [10]. When the cone-and-plate system was utilized to study the effects of FSS on adherent endothelial cells, numerical analysis by finite element method (FEM) showed a minimal region on the plate with a uniform FSS distribution, where FSS was almost constant [11]. Recently, Spruell and Baker developed a high-throughput cone-and-plate system of rotating cone-tipped shafts in a standard 96-well culture plate [12]. Numerical simulation was used to investigate the effects of changing the angular velocity and the gap

* Corresponding author. Department of Mechanics, School of Aerospace Engineering, Beijing Institute of Technology, No. 5 South Zhongguancun Street, Beijing, 100081, PR China.
E-mail address: huobo@bit.edu.cn (B. Huo).

https://doi.org/10.1016/j.compbiomed.2019.01.014
Received 29 September 2018; Received in revised form 16 January 2019; Accepted 19 January 2019

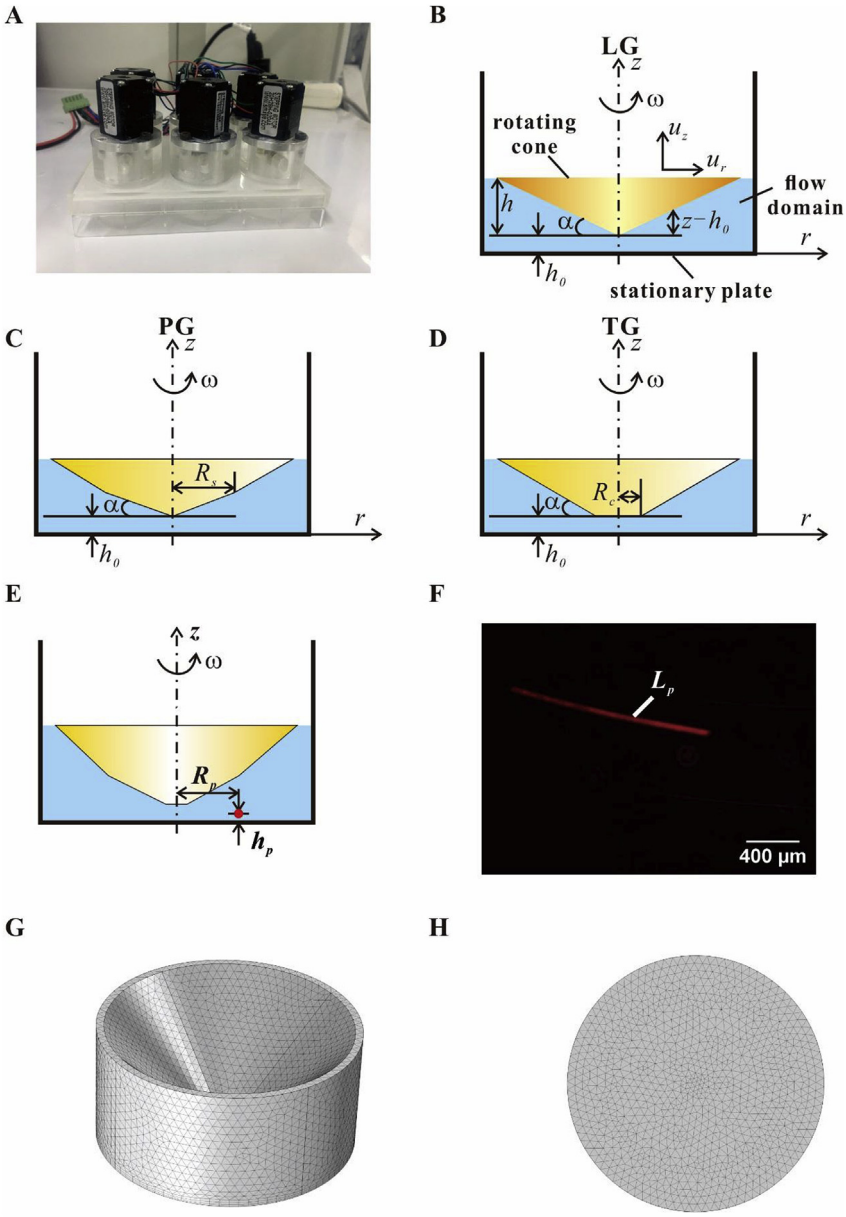

Fig. 1. Cone-and-plate flow chamber for applying FSS on a standard six-well culture plate. (A) Image of the cone-and-plate device. (B–D) Schematic diagram of LG, PG and TG with one-well plate, respectively. (E) A typical image of fluorescent bead's trajectory. (F) The chart showing the location of the fluorescent bead (red dot) during PIV measurement. (G) Side-view mesh and (H) bottom-view mesh of the FEM model.

distance between the cone and the base of the well. It was observed that when the gap distance was larger than 1 μm, FSS displayed a linear distribution along the radial direction and no constant-FSS region was apparent.

Various computational approaches have been applied in order to understand the impact of such devices on overall cell growth. However, these models cannot provide a comprehensive perspective regarding the system dynamics, due to the limitations inherent of the underlying approaches. A novel multi-paradigm modeling platform capable of simulating the bidirectional relationship between cells and their microenvironment has also been demonstrated [13], and Massai et al. developed a versatile bioreactor suitable for suspension cell culture under tunable FSSconditions [13,14].

In this study, we designed a new cone-and-plate flow chamber in a standard six-well culture plate. One significant difference between our device and those previously mentioned is that the cone's generatrix is non-linear. We conducted numerical simulation to optimize the geometric parameters, such as the generatrix shape, gap distance, and cone angle; and also the physical parameters, such as viscosity coefficient and angular velocity. Finally, we conducted an experiment based on particle image velocimetry (PIV) method to validate the distribution of the wall FSS. This newly-designed device may be suitable for exposing cells in a flow field with uniform FSS in a physiological environment.

2. Methods

2.1. Device design

A cone-and-plate device that can be used with a standard six-well culture plate was designed (Fig. 1A), in which six motors were mounted with a polymethyl methacrylate cover and driven to rotate by a motor controller. Each motor was connected to a cone, and the cone's rotation applied shear fluid flow on the cells cultured on the plates. The

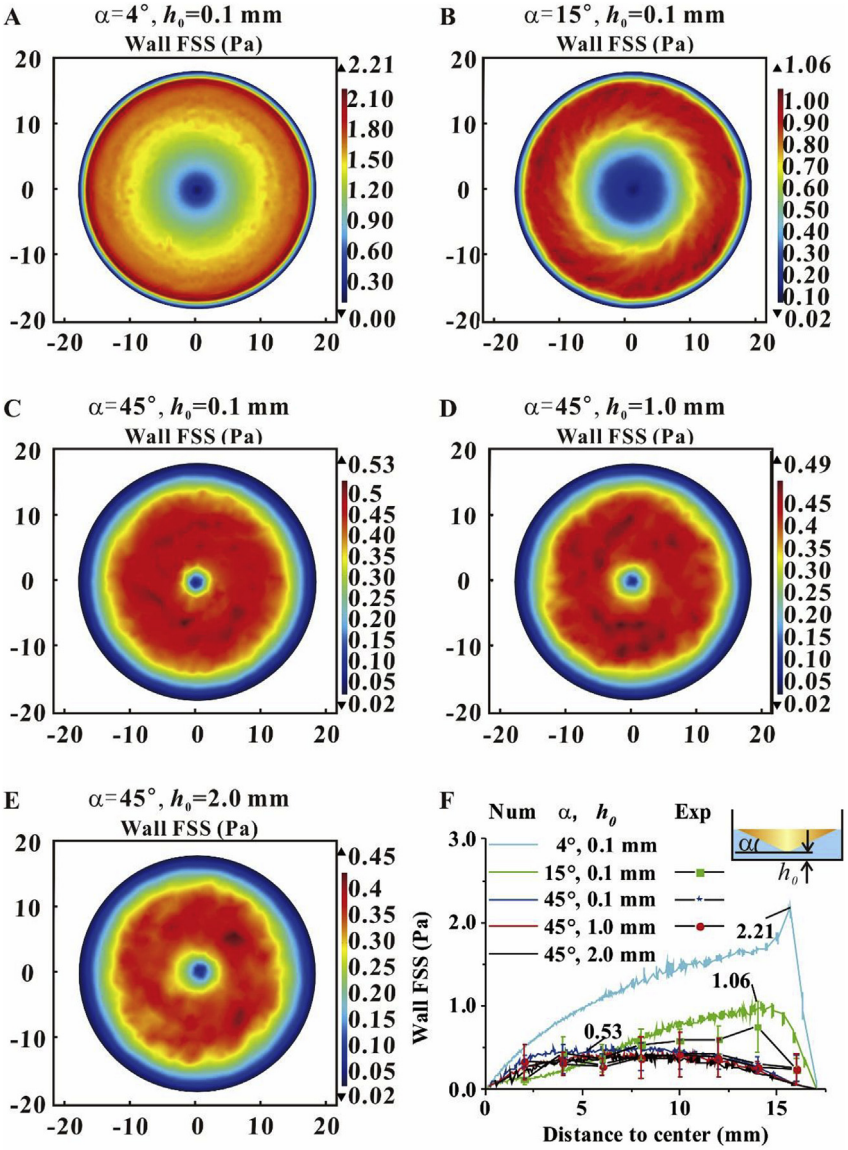

Fig. 2. The effects of geometric parameters on wall FSS profiles. Angular velocity of the cone is 31 rad/s. (A–C) FSS profiles for cone angle of 4°, 15°, and 45°, respectively. (D, E) FSS profiles for gap distances of 1.0 and 2.0 mm, respectively. (F) The relationship between FSS and the distance to center.

Table 1
The parameters of LG for numerical simulation and PIV measurements.

No.	Angular velocity (rad/s)	Viscosity (mPa s)	Gap distance (mm)	Cone angle (°)	Numerical simulation	PIV measurement
1	31	1	0.1	45	✓	✓
2	31	1	0.1	15	✓	✓
3	31	1	0.1	4	✓	–
4	50	1	0.1	45	✓	✓
5	100	1	0.1	45	✓	–
6	31	5	0.1	45	✓	–
7	31	10	0.1	45	✓	–
8	18	1	0.1	0.6	✓	–
9	31	1	1	45	✓	✓
10	31	1	2	45	✓	

schematic diagrams of LG, PG and TG in a one-well plate are shown in Fig. 1B, 1C and 1D, respectively. The radii of the plate and the cone were kept at constant values of 17 mm and 16 mm throughout this study, respectively. For the cone's generatrix, three types of shape parameters were adopted: linear generatrix (LG, $R_s = 0$, $R_c = 0$), polyline generatrix (PG, $R_s \neq 0$, $R_c = 0$), and truncated generatrix (TG, $R_s = R_c \neq 0$). The geometric parameters to be optimized included cone angle α and gap distance h_0 between the cone tip and the plate.

2.2. PIV measurement

To obtain the wall FSS at a different location under varying conditions, PIV was adopted in the present study. PIV is an optical method of flow visualization, used to measure flow direction and the velocity of suspended particles in the fluid. Carboxylate-modified polystyrene fluorescent red particles with 0.4–0.6 μm in diameter were used (Sigma-Aldrich, USA). Initially, 2 mL water was infused into a six-well culture plate, and 2.5 μL fluorescent particles solution was then added and mixed. The particles in the focal plane with 50 μm away from the plate surface were observed (Fig. 1E). The exposure duration is 30 ms and the trajectory of particles was recorded under the excitation light of 515–560 nm in wavelength (Fig. 1F). The trajectory length was measured and then the velocity was calculated by dividing the length by 30 ms. As the density of particles is about 1.045×10^3 kg/m^3, which is similar to water, the measured velocity of fluorescent particles can be assumed to be the local velocity of the fluid. Finally, the wall FSS was

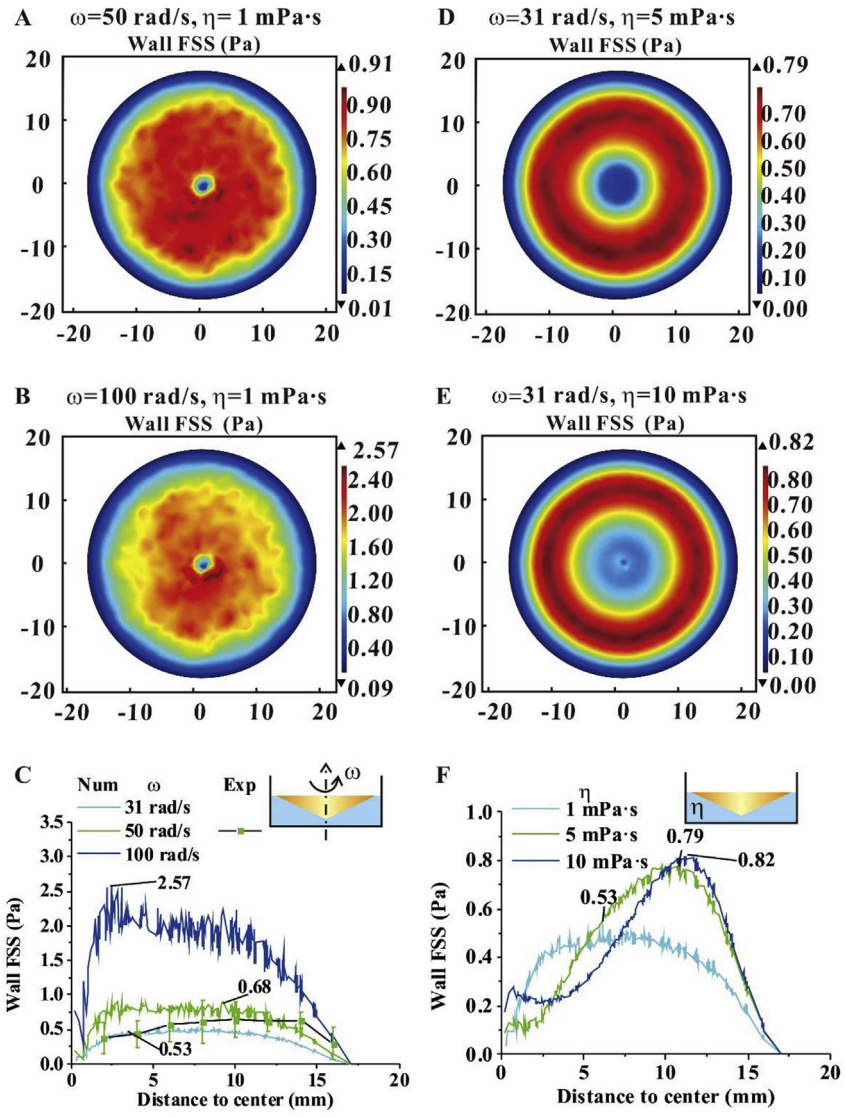

Fig. 3. The effects of physical parameters on wall FSS profiles. (A, B) FSS profiles for angular velocity of 50 and 100 rad/s, respectively, as well as (C) the relationship between FSS and the distance to center. (D, E) FSS profiles for viscosity coefficient of 5 and 10 mPa·s, respectively, and (F) the relationship between FSS and the distance to the center.

computed by dividing the local velocity with the distance of 50 μm.

2.3. Numerical simulation

The flow field was numerically simulated by FEM using the COMSOL Multiphysics software. The Navier–Stokes equations were used to define the flow behavior of viscous fluids. The incompressible flow of a Newtonian fluid was assumed with constant density ρ. The physical parameters to be optimized included viscosity coefficient η and angular velocity ω. The mesh of the FEM model is shown in Fig. 1G and 1H. Tetrahedron mesh was used in this model and 100,000 elements were adopted. To obtain accurate flow field on the bottom surface, we defined three boundary layers. No-slip boundary condition was assumed for all rigid surfaces in the model, and an open boundary condition was used for the upper fluid surface within the well. Sliding wall boundary condition was used for the rotating cone. For steady flow, we solved the equations using an iterative method, and the convergence was identified when the relative tolerance was less than 0.001. MATLAB and Origin software were used for data processing.

2.4. Steady flow case

For the case of steady flow, in the numerical simulations for optimizing the parameters, we adopted the Reynolds number as defined by Sdougos et al. for a cone-and-plate chamber without gap distance [15],

$$\mathrm{Re} = \frac{R^2\omega\alpha^2}{12\nu} \tag{1}$$

where R is the radius of the cone-and-plate chamber and ν is the kinematic viscosity ($\nu = \eta/\rho$). The study demonstrated that laminar flow was observed in the cone-and-plate system with no gap distance when $Re < 0.5$ but turbulence was observed when $Re > 4$. In our study, the Reynolds number used range from 0.03 to 2100. When the case is non-convergent and the residual error is more than 0.001, we used k-ω turbulent model and GEMRS solution to compute, otherwise the laminar flow model was adopted.

The azimuthal turbulence intensities were introduced to indicate the flow case [16],

$$I = \frac{1}{u}\sqrt{\frac{1}{3}(u_r^2 + u_z^2)} \tag{2}$$

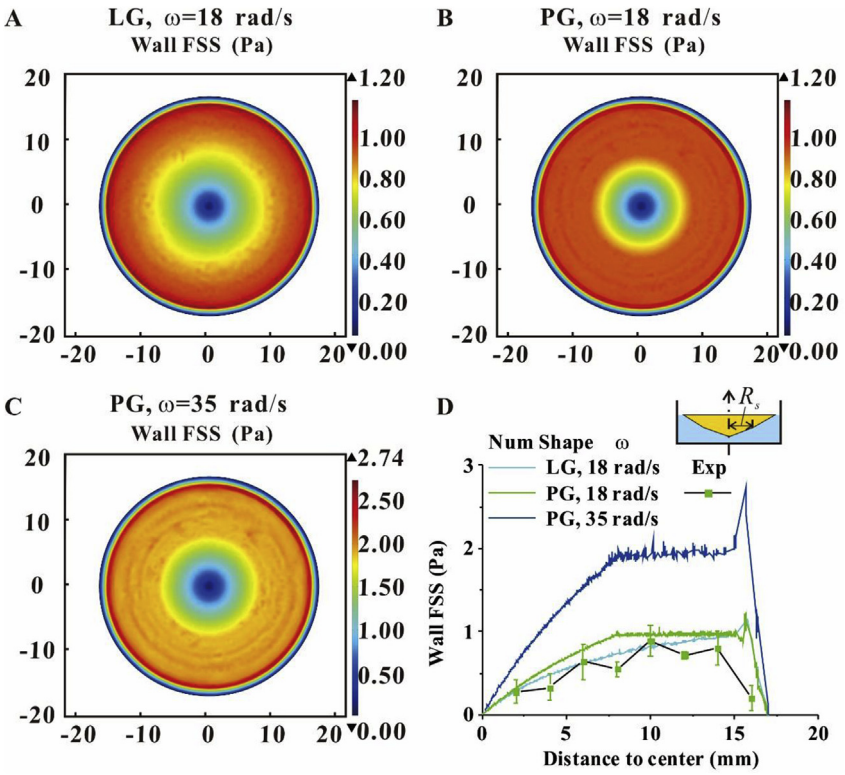

Fig. 4. FSS profile for PG cone compared with LG cone. (A) FSS profiles for LG cone with an angular velocity of 18 rad/s. (B, C) FSS profile for PG cone with angular velocities of 18 and 35 rad/s, respectively. (D) The relationship between FSS and the distance to the center.

Table 2
The parameters of PG for numerical simulation and PIV measurements (h_0 = 0.1 mm).

No.	Angular velocity (rad/s)	Viscosity (mPa·s)	Cone angle (°)	Numerical simulation	PIV measurement
1	0.1	18	1	✓	✓
2	0.1	35	1	✓	–

where u is the total velocity in the cone-plate system, and u_r and u_z are radial and axial velocity respectively.

FSS is calculated according to the following equation,

$$\tau = \eta \frac{dv}{dz} \tag{3}$$

We need to first calculate the shear strain rate $\dot{\gamma} = dv/dz$ along the z direction close to the plate surface based on numerical simulation results, and then FSS was obtained by multiplying with the viscosity coefficient.

3. Results

3.1. Geometric and physical parameters of LG have different effects on FSS distribution

First, we considered the effects of geometric parameters on FSS distribution for the cone with LG. Three different cone angles of 45°, 15°, and 4° and three different gap distances of 0.1 mm, 1 mm, and 2 mm were applied. During the numerical simulation, the viscosity coefficient was 1 mPa·s, and the angular velocity was 31 rad/s. The simulation results showed that for gap distance h_0 = 0.1 mm, and cone angle was 45° (Fig. 2C), a relatively uniform profile of FSS was apparent in most regions of the plate compared with the other two tests where different cone angles were used (Fig. 2A and B), but its value dropped to zero at the center (Fig. 2F). The peak value of FSS corresponding to the tests shown in Fig. 2C–E was approximately 0.5 Pa. When the cone angles were reduced to 15° or 4°, the FSS distribution along the radial direction was not time-invariant, and the maximum value increased to 1.06 or 2.21 Pa, respectively. For the tests where the cone angle was maintained constant at 45°, together with the increase of gap distance, the difference between the profiles of FSS distribution was negligible (Fig. 2C–F). As flow study at the cellular level usually requires high FSS values such as 1–2 Pa in most regions of the plate, the current geometric parameters with linear cone generatrix did not meet the requirements of a biological experiment. PIV measurements were adopted to validate the simulation results with cone angles of 45° or 15°, and a gap distance of 0.1 or 1.0 mm, respectively. The experimental and numerical simulation results gave a similar distribution of wall FSS, i.e. the larger cone angle increased the FSS level but led to non-uniform FSS distribution along the radial direction (Fig. 2F). The parameters for numerical simulation and PIV measurement are shown in Table 1.

We next examined the effects of physical parameters, such as angular velocity and viscosity, on FSS distribution for the case of LG (Fig. 3). During this numerical simulation, the gap distance and cone angle were set at 0.1 mm and 45°, respectively. When the viscosity coefficient was set as a constant value of 1 mPa·s, three different angular velocities of 31 rad/s, 50 rad/s, and 100 rad/s were adopted (Figs. 2C, 3A and 3B, and 3C). The results showed that along with the increase in angular velocity, the peak value of FSS improved from 0.53 Pa to 2.57 Pa, but uniform FSS profile only occurred at low angular velocity of 31 rad/s. The PIV result for 50 rad/s showed a similar distribution of wall FSS with the corresponding numerical result (Fig. 3C). For the case with constant angular velocity of 31 rad/s, along with the

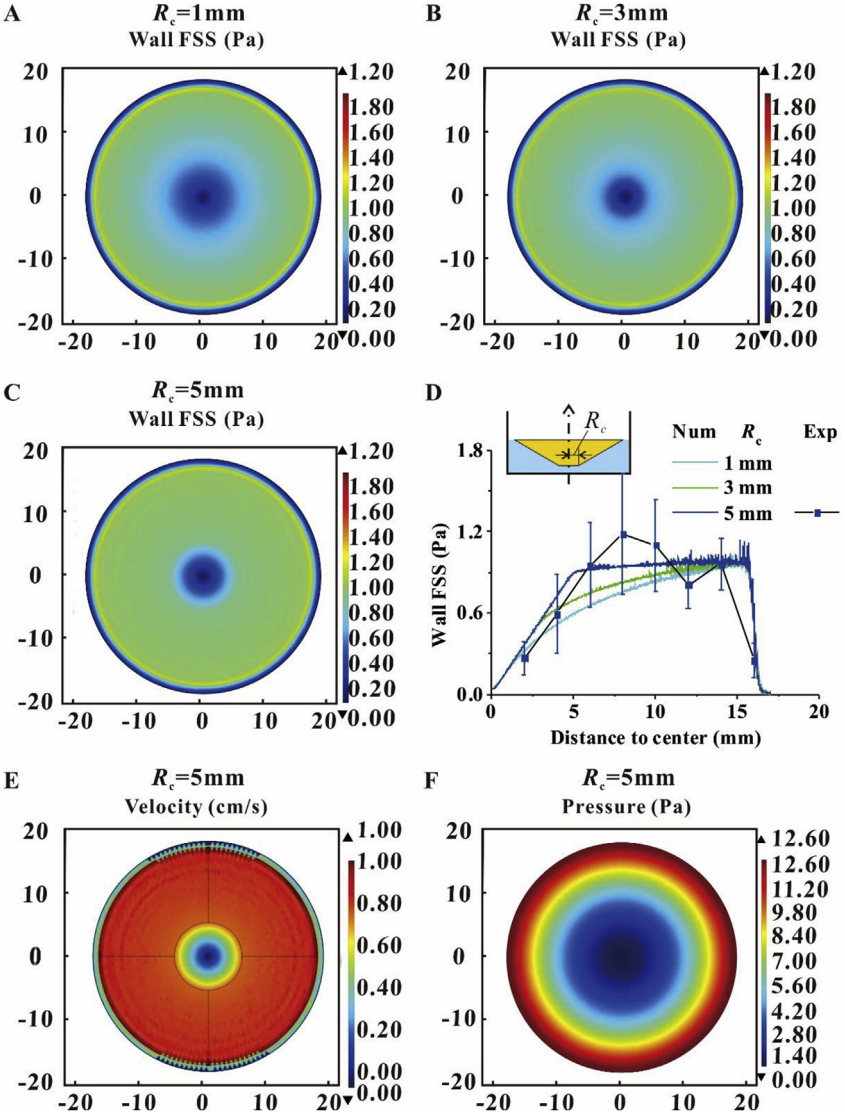

Fig. 5. FSS profile for TG cone. Angular velocity of the cone is 18 rad/s. (A–C) FSS profiles for TG with three radii R_c of 1, 3, and 5 mm, respectively. (D) The relationship between FSS and the distance to center. (E) Velocity profile at 10 μm away from the bottom surface. (F) Pressure profile at the bottom surface.

increase of viscosity coefficient from 1 mPa·s to 10 mPa·s (Figs. 2C, 3D and 3E and 3F), the peak value of FSS increased to 0.82 Pa, but its profile was not radially uniform. Therefore, for the case of LG, adjusting only the physical parameters of angular velocity or viscosity will not change the FSS value, nor will it produce a uniform distribution.

3.2. The shape of the cone's generatrix for PG or TG significantly influences the region with uniform FSS distribution

To broaden the region with uniform FSS distribution and improve the FSS value, the cone with PG was adopted, in which R_s = 8 mm and h_s = 0.05 mm (Fig. 4). During the numerical simulation, parameters h_0 = 0.1 mm, h = 0.2 mm, ω = 18 rad/s, and η = 1 mPas were used. The results showed that compared with LG, PG broaden the region of the FSS distribution uniform and increases the size, from 8.0 mm to 14.8 mm relative to the center, with the value of FSS at the uniform region 1 Pa (Fig. 4A, B, and 4D). Furthermore, after angular velocity was increased to 35 rad/s, the corresponding FSS was enhanced up to 2 Pa (Fig. 4C and D). Moreover, PIV experimental results for angular velocity of 18 rad/s showed that FSS distribution in most region has a similar tendency with numerical simulation but displayed more fluctuation. Furthermore, the FSS level in different locations obtained by PIV measurement is slightly lower than that predicted by FE calculation. The parameters for numerical simulation and PIV measurement are shown in Table 2.

The shape of the cone's generatrix was then changed into TG, with h = 0.2 mm (Fig. 5). During the numerical simulation, parameters were defined as h_0 = 0.1 mm, ω = 18 rad/s, and η = 1 mPa·s. The numerical results indicated that with the increase of R_c value, the region with uniform FSS was significantly enlarged from 5 mm to 15 mm, and its value was also improved to 1 Pa. The fluctuation of FSS distribution was increased in the outer region of the circular plate, especially for higher R_c value (Fig. 5A–D). The wall FSS measured by PIV for R_c = 5 mm increased along with the distance to the center in the region of 0–6 mm and then displayed a fluctuation feature relative to 1 Pa with about 20% difference (Fig. 5D). The distribution of velocity at 10 μm away from the plate revealed a distinct uniform velocity in the region of R_c = 5–15 mm (Fig. 5E), which should be driven by the constant pressure gradient (Fig. 5F).

3.3. Geometric or physical parameters in TG have different influences on FSS and secondary flow

The effects of gap distance and angular velocity on FSS for the TG

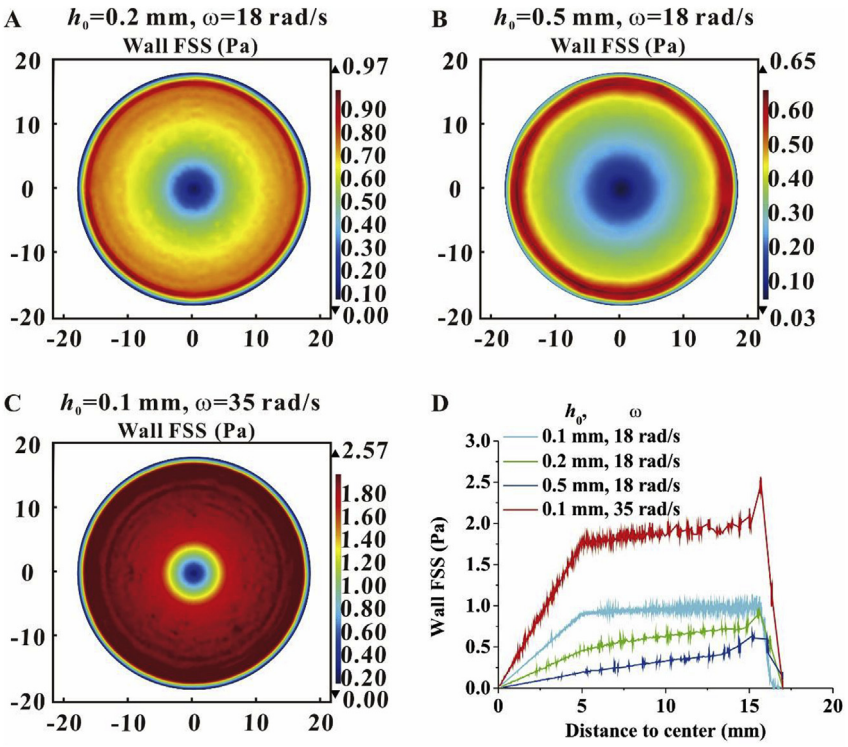

Fig. 6. Effects of gap distance and angular velocity on the wall FSS for TG cone. (A, B) FSS profile for gap distances of 0.2 and 0.5 mm, respectively, with angular velocity of 18 rad/s. (C) FSS profile for gap distance of 0.1 mm and angular velocity of 35 rad/s. (D) The relationship between wall FSS and the distance to the center.

Table 3
The parameters of TG for numerical simulation and PIV measurements.

No.	Gap distance (mm)	Angular Velocity (rad/s)	Viscosity (mPa s)	Truncated radius (mm)	Numerical simulation	PIV measurement
1	0.1	18	1	1	✓	–
2	0.1	18	1	3	✓	–
3	0.1	18	1	5	✓	✓
4	0.2	18	1	5	✓	–
5	0.5	18	1	5	✓	–
6	0.1	35	1	5	✓	–

cone was investigated (Fig. 6). During the numerical simulation, parameters used were $\omega = 18$ rad/s, $\eta = 1$ mPa·s, and $h = 0.2$ mm. Results showed that the decrease in gap distance increased the magnitude of wall FSS. With a gap distance of 0.1 mm, FSS distributed uniformly in a wide region of 5–15 mm along a radial direction, and the magnitude of FSS was 1 Pa. This finding means that the cone needs to be close enough to the plate surface for the fluid between the cone and the plate to be easily driven to flow. With a high angular velocity of 35 rad/s, the magnitude of FSS reached up to 2 Pa in the region of 5–15 mm and the tendency was similar to the results for 18 rad/s. For TG, this region ranged from 5 μm to 15 μm radially, with the area covering 69% of the total area of the bottom surface. For PG, this percentage was only 54%. The parameters for numerical simulation and PIV measurement are shown in Table 3.

For the LG cone with high or low cone angle and angular velocity, and for the optimized PG and TG cones, the flow direction at different locations on the bottom surface is shown in Fig. 7A–D, indicating the occurrence of secondary flow. The average angle of secondary flow for LG was 1.2°–4.7°, which is considerably higher than that of PG and TG. Therefore, TG with larger R_c of 5 mm is beneficial in reducing the secondary flow (Fig. 7E). We then computed azimuthal turbulence intensity with different cone angles, angular velocities and cone type (Fig. 7F). For the LG cone with $\omega = 100$ rad/s, $\alpha = 45°$ ($h = 16$ mm), the average azimuthal turbulence intensity is about 0.1, and for the LG with $\omega = 18$ rad/s, $h = 0.2$ mm as well as for the PG with $\omega = 18$ rad/s, the average azimuthal turbulence intensity is about 0.01, which is significantly lower than LG with high angular velocity and cone angle. For the TG with $\omega = 18$ rad/s, $R_c = 5$ mm, the average azimuthal turbulence intensity is the least among these cones, suggesting that this particular type of cone is beneficial for the reduction of turbulence and providing optimized flow field.

4. Discussion

We constructed a novel cone-and-plate flow chamber based on a standard six-well cell culture plate. The cover with cones and motors was placed on the six-well plate, forming a flow chamber between the cone and the plate. According to traditional fluid mechanics theory, the wall FSS on the plate is constant if there is no gap distance and well boundary existed for the cone with LG. Therefore, the cone-and-plate configuration is suitable for exposing cells cultured on the plate to a uniform and controlled FSS for long-term investigation. Several attempts have been made with this type of device, and the corresponding numerical simulations showed only a minimal region with uniform FSS distribution was formed [11,12]. However, the study of cell mechanics requires a vast region of uniform FSS flow field to ensure that all cells are exposed to the same mechanical environment. In addition, as physiological FSS values are within 0.1–3 Pa [17], a flow chamber

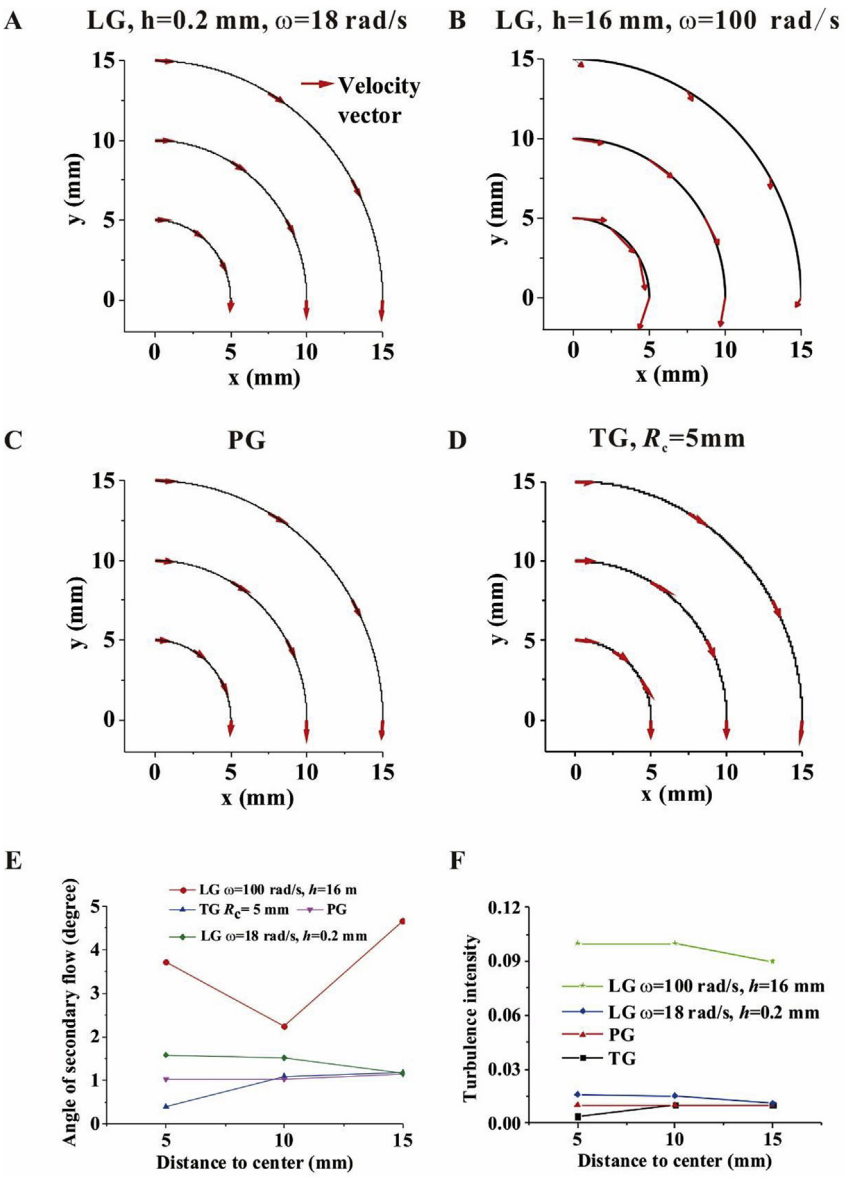

Fig. 7. Secondary flow and turbulence intensity for different types of cones at 10 μm away from the bottom surface. (A, B) For LG with different cone height *h* and angular velocity ω, velocity vectors (red arrows) indicating secondary flow against circumferential direction (black lines) at different radial locations of 5, 10, and 15 mm, respectively. (C, D) Velocity vectors for PG and TG, respectively. (E, F) The relationship between the angle of secondary flow and the azimuthal turbulence intensity with the distance to the center.

should be able to provide enough FSS stimulation on the cells. In this study, we numerically and experimentally investigated the effects of geometric and physical parameters on wall FSS, and optimize them so as to construct a uniform FSS field in an extensive region with sufficiently high magnitude.

First, a traditional cone-and-plate configuration with LG was investigated in this study. The numerical results showed that a large cone angle of 45° and a small angular velocity of 31 rad/s could form a gently varied FSS field but with a relatively low magnitude of approximately 0.2–0.4 Pa, which could not meet the requirement of cell mechanics experiment (Figs. 2F, 3C and 3F). To increase the magnitude of FSS, angular velocity or viscosity coefficient had to be increased, while the cone angle had to be decreased. In the experiments of hemodynamics or blood rheology, dextran is usually used to increase the viscosity of a solution without influencing the biological behaviors of cells [18]. In these cases, however, distinct gradient distribution of FSS along the radial direction will be produced. In previous studies on cone-and-plate, the numerical simulation also demonstrated difficulty in constructing an extensive region with a uniform FSS [11,12]. When a very tiny gap distance down to 1 μm was applied, a uniform FSS region could form, and its magnitude even reached 5 Pa [12]. However, for a mechanical device, making and retaining such a minute distance between the cone's tip and the plate surface is extremely difficult. Therefore, we had to find an alternative way to solve this problem.

In the current study, two types of cones with PG and TG were used. Our results demonstrated that both were able to produce a uniform FSS distribution, although the region with uniform FSS for TG was considerably larger than the one for PG (Figs. 4D and 5D). More importantly, the magnitude of wall FSS in the uniform region for TG was 1 Pa or 2 Pa at different angular velocities of 18 rad/s or 35 rad/s, respectively, as well as a gap distance of 0.1 mm, demonstrating that this device is suitable to be used. This modification of TG or PG resulted in a large radius of the cone's surface, i.e., with higher linear velocity, thus the plate surface is in closer proximity to the cone compared to that with a small radius. Therefore, the fluid between the cone and the plate surface was quickly driven to flow. Additionally, as FSS distribution

was sensitive to gap distance, the vertical location of the cone should be accurately controlled during experiments.

The secondary flow phenomena in a cone-and-plate system was discovered previously [10]. Some theoretical studies demonstrated that at a sufficiently low shear rate, the secondary flow was negligible, and the primary flow along the circumferential direction provided an excellent approximation to the flow [19,20]. Another study revealed that the case of secondary flow should be dependent on a precise defined Reynolds number $\mathrm{Re} = \rho R^2\omega\alpha^2/(12\eta)$, or $\mathrm{Re} = \rho\omega h^2/(12\eta)$ if the cone angle is very minute (see Eq. (1)) [15]. The type of flow was found to be a laminar flow when *Re* was lower than 0.5, and secondary flow would occur when $Re > 0.5$. Furthermore, turbulence was found for $Re > 4$. According to this definition of *Re*, for the cases with high angular velocity, low viscosity, and especially high cone height, the Reynolds number in the present study may be as large as 2.1×10^3 for the LG cone, thus turbulence might cause high fluctuation of wall FSS distribution (Figs. 2F, 3C and 3F). For the newly designed PG and TG cones, the cones' height was reduced to 0.2 mm, and the distance between the cones' surface location with high linear velocity and the plate surface was also decreased. In these cases, the Reynolds number was less than 0.1, such that the fluid flow could be treated as a laminar flow; thus, the wall FSS distribution produced was uniform (Figs. 5D and 6D).

In conclusion, a new cone-and-plate flow chamber with TG was designed in this study. The results of numerical simulation and PIV measurement showed that the region with uniform wall FSS on the plate was significantly larger than that of the traditional cone-and-plate system with LG. Moreover, the magnitude of FSS in the cone-and-plate flow chamber with TG was markedly higher than that for the conventional method system. Thus, considering that this device can be easily used with a standard six-well culture plate, it should become a powerful tool for *in vitro* experiment of cell mechanics.

Conflicts of interest

There are no conflicts to declare.

Acknowledgement

This work was supported by the National Natural Science Foundation of China [11572043 and 11372043 (BH)].

Appendix A. Supplementary data

Supplementary data to this article can be found online at https://doi.org/10.1016/j.compbiomed.2019.01.014

References

[1] W.W. Yan, B. Cai, Y. Liu, et al., Effects of wall shear stress and its gradient on tumor cell adhesion in curved microvessels, Biomechanics Model. Mechanobiol. 11 (5) (2012) 641–653.
[2] C. Wittkowske, G.C. Reilly, D. Lacroix, et al., In vitro bone cell models: impact of fluid shear stress on bone formation, Front. Bioeng. Biotechnol. 4 (2016) 87.
[3] C. Price, X.Z. Zhou, W. Li, et al., Real-time measurement of solute transport within the lacunar-canalicular system of mechanically loaded bone: direct evidence for load-induced fluid flow, J. Bone Miner. Res. 26 (2) (2011) 277–285.
[4] L.Y. Wang, Y.L. Wang, Y.F. Han, et al., In situ measurement of solute transport in the bone lacunar-canalicular system, Proc. Natl. Acad. Sci. U. S. A 102 (33) (2005) 11911–11916.
[5] H. Kang, J. Liu, A. Sun, et al., Vascular smooth muscle cell glycocalyx mediates shear stress-induced contractile responses via a Rho kinase (ROCK)-myosin light chain phosphatase (MLCP) pathway, Sci. Rep. 7 (2017) 42092.
[6] R.M. Delaine-Smith, B. Javaheri, J.H. Edwards, et al., Preclinical models for in vitro mechanical loading of bone-derived cells, BoneKEy Rep. 4 (2015) 728.
[7] L.H. Wu, H.C. Chang, P.C. Ting, et al., Laminar shear stress promotes mitochondrial homeostasis in endothelial cells, J. Cell. Physiol. 233 (6) (2017) 5058–5069.
[8] T.G. Vankooten, J.M. Schakenraad, H.C. Vandermei, et al., Development and use of a parallel-plate flow chamber for studying cellular adhesion to solid-surfaces, J. Biomed. Mater. Res. 26 (6) (1992) 725–738.
[9] M. Mooney, R.H. Ewart, The conicylindrical viscosimeter, Physics 5 (1934) 350–354.
[10] D.B. Cox, Radial flow in cone-plate viscosimeter, Nature 193 (4816) (1962) 670.
[11] M.H. Buschmann, P. Dieterich, N.A. Adams, et al., Analysis of flow in a cone-and-plate apparatus with respect to spatial and temporal effects on endothelial cells, Biotechnol. Bioeng. 89 (5) (2005) 493–502.
[12] C. Spruell, A.B. Baker, Analysis of a high-throughput cone-and-plate apparatus for the application of defined spatiotemporal flow to cultured cells, Nature 110 (6) (2013) 1782–1793.
[13] H. Kaul, Z.F. Cui, Y. Ventikos, A multi-paradigm modeling framework to simulate dynamic reciprocity in a bioreactor, PLoS One 8 (3) (2013).
[14] D. Massai, G. Isu, D. Madeddu, et al., A versatile bioreactor for dynamic suspension cell culture. Application to the Culture of Cancer Cell Spheroids (vol 11, e0154610, 2016), PLoS One 11 (6) (2016).
[15] H.P. Sdougos, S.R. Bussolari, C.F. Dewey, Secondary flow and turbulence in a cone-and-plate device, J. Fluid Mech. 138 (1984) 379–404 (JAN).
[16] S. Einav, C.F. Dewey, H. Hartenbaum, Cone-and-plate apparatus - a compact system for studying well-characterized turbulent-flow fields, Exp. Fluid 16 (3–4) (1994) 196–202.
[17] C.L. Liu, S. Li, B.H. Ji, et al., Flow-induced migration of osteoclasts and regulations of calcium signaling pathways, Cell. Mol. Bioeng. 8 (1) (2015) 213–223.
[18] Y.J. Kang, Periodic and simultaneous quantification of blood viscosity and red blood cell aggregation using a microfluidic platform under in-vitro closed-loop circulation, Biomicrofluidics 12 (2) (2018) 024116.
[19] C.F. Dewey, S.R. Bussolari, M.A. Gimbrone, et al., The dynamic response of vascular endothelial cells to fluid shear stress, J. Biomech. Eng. Trans. Asme 103 (3) (1981) 177–185.
[20] M.E. Fewell, J.D. Hellums, The Secondary flow of Newtonian fluids in cone-and-plate viscometers, Trans. Soc. Rheol. 21 (4) (1977) 535–565.